Cardiac-specific overexpression of AT1 receptor mutant lacking $G_\alpha q/G_\alpha i$ coupling causes hypertrophy and bradycardia in transgenic mice

Peiyong Zhai,[1] Mitsutaka Yamamoto,[1] Jonathan Galeotti,[1] Jing Liu,[1] Malthi Masurekar,[1] Jill Thaisz,[1] Keiichi Irie,[1] Eric Holle,[2] Xianzhong Yu,[2] Sabina Kupershmidt,[3] Dan M. Roden,[4] Thomas Wagner,[2] Atsuko Yatani,[1] Dorothy E. Vatner,[1] Stephen F. Vatner,[1] and Junichi Sadoshima[1]

[1]Cardiovascular Research Institute, Department of Cell Biology and Molecular Medicine, University of Medicine and Dentistry of New Jersey, New Jersey Medical School, Newark, New Jersey, USA. [2]Oncology Research Institute, Greenville, South Carolina, USA. [3]Department of Anesthesiology and [4]Department of Pharmacology, Vanderbilt University School of Medicine, Nashville, Tennessee, USA.

Ang II type 1 (AT1) receptors activate both conventional heterotrimeric G protein–dependent and unconventional G protein–independent mechanisms. We investigated how these different mechanisms activated by AT1 receptors affect growth and death of cardiac myocytes in vivo. Transgenic mice with cardiac-specific overexpression of WT AT1 receptor (AT1-WT; Tg-WT mice) or an AT1 receptor second intracellular loop mutant (AT1-i2m; Tg-i2m mice) selectively activating $G_\alpha q/G_\alpha i$-independent mechanisms were studied. Tg-i2m mice developed more severe cardiac hypertrophy and bradycardia coupled with lower cardiac function than Tg-WT mice. In contrast, Tg-WT mice exhibited more severe fibrosis and apoptosis than Tg-i2m mice. Chronic Ang II infusion induced greater cardiac hypertrophy in Tg-i2m compared with Tg-WT mice whereas acute Ang II administration caused an increase in heart rate in Tg-WT but not in Tg-i2m mice. Membrane translocation of PKCε, cytoplasmic translocation of $G_\alpha q$, and nuclear localization of phospho-ERKs were observed only in Tg-WT mice while activation of Src and cytoplasmic accumulation of phospho-ERKs were greater in Tg-i2m mice, consistent with the notion that $G_\alpha q/G_\alpha i$-independent mechanisms are activated in Tg-i2m mice. Cultured myocytes expressing AT1-i2m exhibited a left and upward shift of the Ang II dose-response curve of hypertrophy compared with those expressing AT1-WT. Thus, the AT1 receptor mediates downstream signaling mechanisms through $G_\alpha q/G_\alpha i$-dependent and -independent mechanisms, which induce hypertrophy with a distinct phenotype.

Introduction

Ang II is an important terminal effector of the renin-angiotensin system (RAS), which plays a critical role in the regulation of blood pressure and volume homeostasis (1). Enhanced activity of RAS is associated with various cardiovascular diseases, such as hypertension, cardiac hypertrophy, and heart failure (2–4). Ang II is produced in the heart through local RAS and plays a critical role in mediating load-induced cardiac hypertrophy and cardiac remodeling (5, 6). These pathologic effects of Ang II on the heart are primarily mediated by the Ang II type 1 (AT1) receptor, a 7 transmembrane G protein–coupled receptor (GPCR) (7). Thus, elucidating the signaling mechanism of the AT1 receptor is important for the development of fundamental treatment for cardiac hypertrophy and heart failure.

Nonstandard abbreviations used: ANF, atrial natriuretic factor; ASA, α-skeletal actin; AT1, Ang II type 1; AT1-i2m, AT1 receptor second intracellular loop mutant; AT1-WT, WT AT1 receptor; AV, atrioventricular; AVN, AV node; BW, body weight; GPCR, G protein–coupled receptor; GTPγS, guanosine 5′-*O*-(3-thiotriphosphate); HR, heart rate; I_{Ca}, L-type Ca^{2+} channel current; LVEDD, LV end-diastolic dimension; LVESD, LV end-systolic dimension; LVW, LV weight; NTg, non-Tg; PEA-15, phosphoprotein enriched in astrocytes; qPCR, quantitative PCR; RAS, renin-angiotensin system; Tg-i2m mice, transgenic mice with cardiac-specific overexpression of AT1-i2m; Tg-WT mice, transgenic mice with cardiac-specific overexpression of AT1-WT; TL, tibia length.

Conflict of interest: The authors have declared that no conflict of interest exists.

Citation for this article: *J. Clin. Invest.* **115**:3045–3056 (2005). doi:10.1172/JCI25330.

The signaling mechanism of the AT1 receptor is traditionally described as dependent on heterotrimeric G proteins (8). The AT1 receptor activates phospholipase Cβ via $G_\alpha q$ proteins. This causes generation of inositol trisphosphate and diacylglycerol, which in turn causes release of calcium from intracellular calcium stores and activation of PKC, respectively (8). The AT1 receptor also couples to $G_\alpha i$, thereby regulating adenylyl cyclase (9). Previous studies from our laboratory as well as from others have suggested, however, that the AT1 receptor also activates unconventional signaling mechanisms, such as $G_\alpha q/G_\alpha i$-independent and/or heterotrimeric G protein–independent signaling mechanisms (10–17). In many cases, protein-protein interaction between the specific amino acid sequence in the AT1 receptors and intracellular signaling molecules plays an important role in mediating these unique signaling mechanisms (reviewed in refs. 7, 18). For example, we have previously shown that an AT1 receptor having mutations in the second intracellular DRY motif lacks heterotrimeric G protein coupling but still mediates activation of Src and ERK (16). The cytoplasmic domain of the AT1 receptor physically interacts with intracellular signaling molecules, including SHP-2, phospholipase Cγ, and JAK2 (19–22). The conserved YIPP motif in the carboxyl terminus domain of the AT1 receptor interacts with SHP-2, which in turn plays an essential role in mediating activation of the JAK/STAT pathway and EGF receptor (17, 22). AT1 receptors also associate with novel signaling molecules, such as AT1 receptor–associated protein (ATRAP), which in turn affects Ang II–induced cell growth

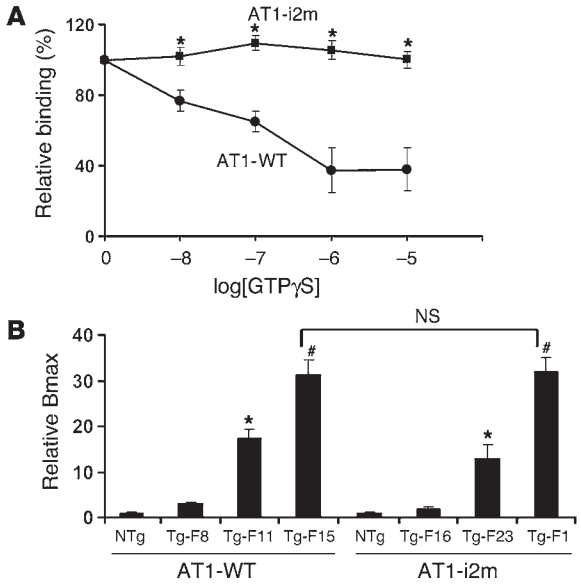

Figure 1
AT1 receptor binding assays. (**A**) Effects of GTPγS on ^{125}I-Ang II binding to the membrane fraction of cardiac myocytes overexpressing AT1-i2m or AT1-WT. *P < 0.01 compared with AT1-WT. (**B**) Radioligand binding assays. Tg-WT (line 15, n = 5) and Tg-i2m mice (line 1, n = 7) had similar levels of AT1 receptor expression. The maximum binding (Bmax; fmol/mg protein) for NTg, Tg-WT (line 15), and Tg-i2m mice (line 1) was 9.0 ± 0.7, 283.3 ± 9.2, and 287.5 ± 13.7, respectively. The dissociation constant (Kd) (nM) for NTg, Tg-WT (line 15), and Tg-i2m mice (line 1) was 0.77 ± 0.13, 0.77 ± 0.19, and 0.79 ± 0.16, respectively. There was no significant difference in AT1 receptor expression between Tg-WT (line 15) and Tg-i2m mice (line 1). Tg-F8, Tg mice derived from the founder number 8 (line 8). *P < 0.01, #P < 0.001 compared with NTg mice. Experiments were conducted 4 and 3 times for **A** and **B**, respectively.

responses in HEK293 cells (23). These sequence-specific signaling mechanisms allow the AT1 receptor to generate unique downstream signaling mechanisms and possibly explain the versatility of AT1-receptor signaling (18).

Previous studies regarding the signaling mechanisms of cardiac hypertrophy have suggested that each signaling mechanism affects cardiac hypertrophy differently (24). For example, activation of $G_\alpha q$ causes hypertrophy with cardiac dysfunction (25) while stimulation of PI3K and ERKs causes well-compensated forms of hypertrophy (26, 27). Since GPCRs, including AT1 receptors, have versatile signaling functions, their downstream signaling could mediate a wide variety of effects upon cardiac phenotype associated with hypertrophy. Although AT1 receptors are able to transmit downstream signaling mechanisms through unconventional signaling mechanisms, whether or not such signaling mechanisms stimulated by the AT1 receptor are able to affect growth and death of the heart remains to be elucidated in vivo. Our goal in this study was to elucidate whether the previously identified $G_\alpha q$- or $G_\alpha i$-independent signaling mechanism of the AT1 receptor is able to mediate hypertrophy in the heart. We here report that activation of the $G_\alpha q$- or $G_\alpha i$-independent signaling mechanism by the AT1 receptor indeed induces hypertrophy with a unique cardiac phenotype in vivo.

Results

Generation of Tg-WT and Tg-i2m mice. Receptor interaction with heterotrimeric G proteins was evaluated by measuring ^{125}I-Ang II binding in the presence of guanosine 5′-*O*-(3-thiotriphosphate) (GTPγS), which shifts GPCRs from a high-affinity state to a low-affinity state. Since this shift is considered an indicator of effective interaction of the receptor with heterotrimeric G proteins (28), we examined the effect of GTPγS on ^{125}I-Ang II binding to the WT AT1 receptor (AT1-WT) and an AT1 receptor second intracellular loop mutant (AT1-i2m). AT1-WT and AT1-i2m were overexpressed in cultured cardiac myocytes, and the membrane fraction was prepared. As shown in Figure 1A, GTPγS decreased Ang II binding to AT1-WT in a dose-dependent manner. By contrast, Ang II binding to AT1-i2m was not affected by GTPγS even at 10^{-5} M, suggesting that AT1-i2m lacks heterotrimeric G protein coupling in cardiac myocytes, consistent with previous results in other cell types (16, 29).

In order to examine the in vivo function mediated by heterotrimeric G protein–independent mechanisms, we developed transgenic mice with cardiac-specific overexpression of AT1-WT (Tg-WT mice) and AT1-i2m (Tg-i2m mice). Cardiac tissue AT1 receptor expression was assessed by radioligand binding assays. Expression of the AT1 receptor in the heart was significantly increased in both Tg-WT and Tg-i2m mice. In the 3 mouse lines examined, the level of AT1 receptor expression in LV occurred in the order of lines 15, 11, and 8 (with line 15 the highest) in Tg-WT mice and lines 1, 23, and 16 in Tg-i2m mice (with line 1 the highest) (Figure 1B). AT1-receptor expression in line 15 of Tg-WT mice was not significantly different from that in line 1 of Tg-i2m mice (Figure 1B).

Tg-i2m mice have greater cardiac hypertrophy than Tg-WT mice. Both ventricles and atria of the heart were enlarged in Tg-WT and Tg-i2m mice (Figure 2, B and D). The LV weight/body weight (LVW/BW) and LVW/tibia length (LVW/TL) were significantly increased in both Tg-WT and Tg-i2m mice compared with non-TG (NTg) mice (Figure 2E and Table 1). Interestingly, LVW/BW and LVW/TL of Tg-i2m mice were significantly greater than those of Tg-WT mice

Table 1
Postmortem pathologic measurements of Tg-WT and Tg-i2m mice

	AT1-WT (founder no. 15)		AT1-i2m (founder no. 1)	
	NTg	Tg	NTg	Tg
n	10	11	16	13
Age (d)	379 ± 37.2	349 ± 46.1	335 ± 36.1	333.1 ± 39.1
BW (g)	31.2 ± 2.0	33.1 ± 2.0	29.7 ± 1.0	30.5 ± 1.1
TL (mm)	19.0 ± 0.4	19.4 ± 0.3	19.5 ± 0.2	19.4 ± 0.3
LV (mg)	91.8 ± 6.0	110.5 ± 6.8[A]	94.7 ± 4.7	134.8 ± 5.4[B,C]
RV (mg)	24.8 ± 1.5	32.5 ± 2.0[A]	22.3 ± 1.7	38.2 ± 1.9[B,C]
LV/BW	2.94 ± 0.06	3.49 ± 0.10[D]	3.17 ± 0.09	4.51 ± 0.24[B,C]
Lung/BW	5.06 ± 0.34	4.81 ± 0.25	6.0 ± 0.2	5.7 ± 0.4
Liver/BW	45.5 ± 1.7	45.0 ± 2.9	46.7 ± 1.5	46.7 ± 1.3
LV/TL	4.45 ± 0.28	5.83 ± 0.29[B]	4.83 ± 0.23	6.75 ± 0.27[B,C]
Lung/TL	8.89 ± 0.16	8.74 ± 0.22	9.03 ± 0.30	8.78 ± 0.62
Liver/TL	81.67 ± 5.67	82.96 ± 8.09	70.32 ± 1.64	68.28 ± 1.97

[A]P < 0.01 and [B]P < 0.0001 compared with corresponding NTg mice; [C]P < 0.05 compared with Tg-WT mice; [D]P < 0.05 compared with corresponding NTg mice.

(Figure 2E). With increasing levels of AT1 receptor expression, the increase in LVW/BW in Tg-i2m mice was significantly greater than that in Tg-WT mice (Figure 2F; complete data set showing postmortem analyses of Tg-WT and Tg-i2m mice can be found in Supplemental Tables 1 and 2; supplemental material available online with this article; doi:10.1172/JCI25330DS1). Thus, Tg-i2m mice developed greater cardiac hypertrophy than Tg-WT mice at each level of AT1 receptor expression. Myocyte size was measured as cell capacitance (which is proportional to the cell surface area). Both ventricular and atrial myocytes isolated from Tg-i2m mice were significantly larger than those from NTg mice (Figure 2G), confirming the occurrence of hypertrophy at the myocyte level in Tg-i2m mice. Ventricular myocytes isolated from Tg-i2m mice were significantly larger than those from Tg-WT mice (Figure 2G). In order to examine whether AT1-i2m has direct effects upon hypertrophy, cardiac myocytes were transduced with adenovirus harboring LacZ, AT1-WT, or AT1-i2m and cultured in serum-free conditions. We confirmed that similar levels of AT1 receptors were overexpressed by receptor-binding assays (Supplemental Figure 1). Ang II–induced increases in protein content were enhanced in AT1-WT and AT1-i2m transduced myocytes. Greater increases in protein content were observed in AT1-i2m–expressing myocytes than in AT1-WT–expressing myocytes. Interestingly, increases in the protein content were induced at lower doses of Ang II in AT1-i2m–expressing cells (Figure 2H).

Expression of hypertrophy-associated genes was quantitated by quantitative PCR (qPCR). With increasing levels of AT1 receptor expression, there was a dose-dependent increase in mRNA expression of atrial natriuretic factor (ANF) and α-skeletal actin (ASA), fetal-type genes, in both Tg-WT and Tg-i2m mice (Figure 3, A and B). mRNA expression of ANF and ASA was significantly higher in Tg-i2m than in Tg-WT mice (Figure 3, A and B). Taken together, these data indicate that overexpression of AT1-i2m induces more severe cardiac hypertrophy than that of AT1-WT.

Echocardiographic measurements indicated that both Tg-WT and Tg-i2m mice showed increased LV end-diastolic dimensions (LVEDDs) and LV end-systolic dimensions (LVESDs) compared with corresponding NTg mice (Table 2). The LVEDDs and LVESDs in Tg-i2m mice were significantly greater than those in Tg-WT mice. These data indicate that Tg-i2m mice have a greater enlargement of the LV chamber than Tg-WT mice.

Tg-i2m mice have more severe bradycardia and reduced cardiac function compared with Tg-WT mice. At 10–12 days, the heart rates (HRs) of Tg-WT and Tg-i2m mice were not significantly different from those of corresponding NTg mice (Table 3). At about 22 days, how-

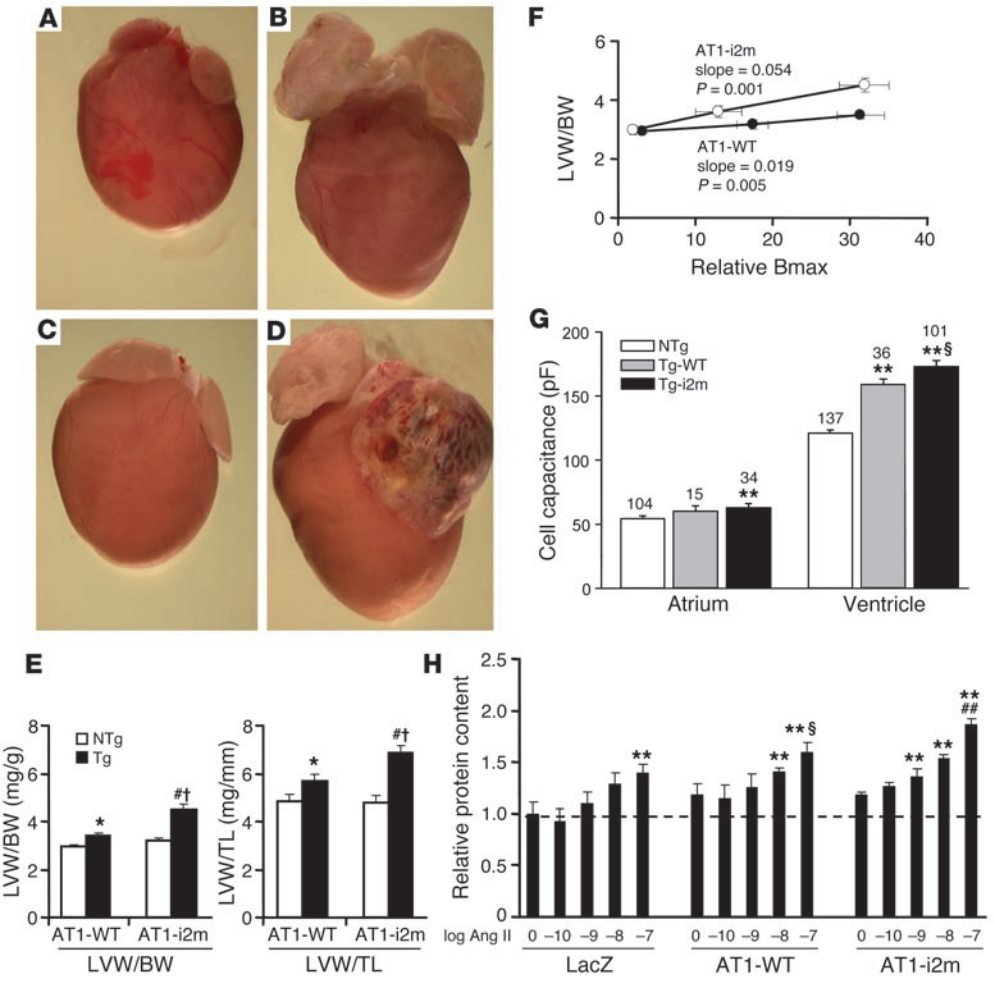

Figure 2

Cardiac hypertrophy in Tg-WT (line 15) and Tg-i2m mice (line 1). (**A**–**D**) Hearts from age-matched nontransgenic littermates for Tg-WT (NTg-WT) (**A**), Tg-WT (**B**), NTg-i2m (**C**), and Tg-i2m mice (**D**) are shown. (**E**) Indices of LV hypertrophy, LVW/BW and LVW/TL, are shown (NTg-WT, $n = 10$; Tg-WT, $n = 11$; NTg-i2m, $n = 15$; Tg-i2m, $n = 16$). $^{*}P < 0.01$, $^{\#}P < 0.0001$ compared with NTg mice. $^{\dagger}P < 0.01$ compared with Tg-WT mice. (**F**) The relationship between AT1 receptor expression and LVW/BW reveals a dose-dependent increase in cardiac hypertrophy in both Tg-WT and Tg-i2m mice (Tg-WT, line 8, $n = 6$, line 11, $n = 4$, line 15, $n = 5$; Tg-i2m, line 16, $n = 6$, line 23, $n = 4$, line 1, $n = 7$). The slope of the relationship in Tg-i2m is 3 times that of Tg-WT mice. (**G**) Average cell capacitance measured in atrial and ventricular myocytes isolated from NTg, Tg-WT, and Tg-i2m mice. Numbers correspond to total number of cells measured. $^{**}P < 0.05$ vs. NTg; $^{\S}P < 0.05$ vs. Tg-WT. Data points are from 8 NTg, 7 Tg-WT, and 9 Tg-i2m mice. (**H**) Protein content of neonatal rat cardiac myocytes transduced with adenovirus harboring LacZ, AT1-WT, or AT1-i2m, with or without various concentrations of Ang II stimulation. The protein content obtained from LacZ transduced myocytes without Ang II stimulation was designated as 1. $^{**}P < 0.05$ vs. LacZ without Ang II. $^{\S}P < 0.05$ vs. LacZ 10^{-7} M Ang II. $^{\#\#}P < 0.05$ vs. AT1-WT 10^{-7} M Ang II. Experiments were conducted in triplicate 3 times.

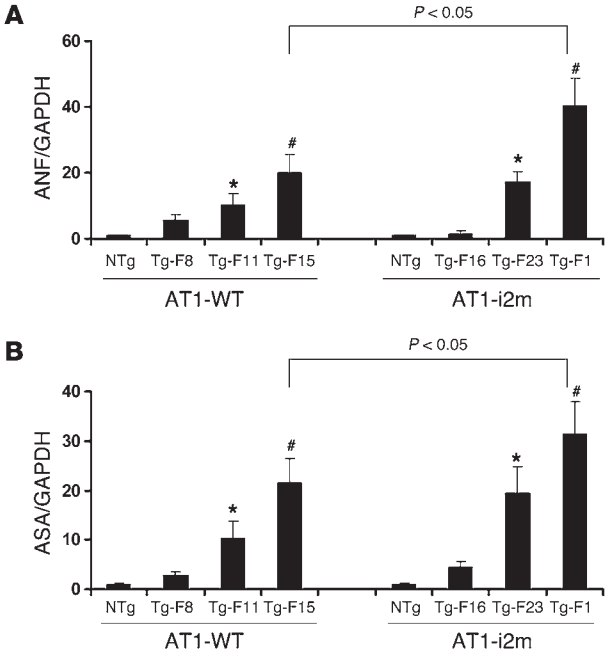

Figure 3
Fetal-type gene expression. Expression of ANF (**A**) and ASA (**B**) in LVs from Tg-WT (line 8, $n = 6$, line 11, $n = 4$, line 15, $n = 5$) and Tg-i2m mice (line 16, $n = 6$, line 23, $n = 4$, line 1, $n = 7$). There was a dose-dependent increase in the expression of ANF and ASA in both Tg-WT and Tg-i2m mice with significantly more ANF and ASA being expressed in Tg-i2m mice. $^{*}P < 0.01$, $^{\#}P < 0.001$ compared with NTg mice.

ever, the HRs of both Tg-WT and Tg-i2m mice were significantly slower than that of corresponding NTg mice (Table 3). The HR of Tg-i2m mice was significantly slower than that of Tg-WT mice at 22 days ($P < 0.005$). ECG showed that Tg-WT mice developed second-degree atrioventricular (AV) block with normal QRS duration while Tg-i2m mice developed complete AV block with significantly widened QRS interval (Figure 4A and Table 4). Bradycardia and conduction abnormality were observed in both Tg-WT and Tg-i2m adult mice as well. Analysis of the relationship between the level of AT1-receptor expression and the HR revealed that there was a significant dose-dependent decrease in HR in Tg-i2m but not in Tg-WT mice (Figure 4, B and C). A 4-week treatment with losartan, an AT1 receptor antagonist, starting at 4 weeks failed to increase HR despite significant reversal of cardiac hypertrophy in Tg-i2m mice (Supplemental Figure 2).

No overt heart failure developed in either Tg-WT or Tg-i2m mice, as evidenced by the fact that neither premature death nor increases in lung or liver weight were observed in either group during our follow-up for 18 months. Echocardiographically measured LV ejection fraction (LVEF) and LV fractional shortening (LVFS) were slightly but significantly lower in both Tg-WT and Tg-i2m mice than in corresponding NTg mice (Table 2). LV $+dP/dt$ and $-dP/dt$ of Tg-WT and Tg-i2m mice were significantly lower than those of corresponding NTg mice, and LV $+dP/dt$ and $-dP/dt$ of Tg-i2m mice were significantly lower than those of Tg-WT mice (Table 5). LV end-diastolic pressure (LVEDP) of Tg-WT mice was not significantly different from that of NTg mice, while that of Tg-i2m mice was significantly higher than that of both NTg and Tg-WT mice (Table 5). This impaired LV function in Tg-i2m was not due to bradycardia alone because ventricular pacing (500/min) failed to normalize $+dP/dt$ or $-dP/dt$ (Figure 4D). These data indicate that overexpression of AT1-WT or AT1-i2m causes impaired LV function with overexpression of AT1-i2m resulting in a greater reduction in LV function than that of AT1-WT.

To identify a possible cause of bradycardia and AV block, histological analyses were conducted. In 4-chamber view cardiac sections, the AV node (AVN) in Tg-i2m mice was poorly developed compared with that in NTg or Tg-WT mice (Supplemental Figure 3). In order to confirm that Tg-i2m mice possess a poorly developed AVN, we crossed Tg-i2m and $MinK^{+/-}$ mice, and whole heart β-galactosidase staining was conducted (30). The spatial expression of MinK in the adult mouse heart is, for the most part, coincident with the conduction tissues. Thus, the cardiac conduction system in $MinK^{+/-}$ mice, in which the *MinK* gene was disrupted by knock-in of the *lacZ* gene, can be labeled with β-galactosidase staining (30). In $MinK^{+/-}$ mouse hearts, β-galactosidase staining of the AVN was clearly observed. On the other hand, in the hearts of $MinK^{+/-}$ Tg-i2m mice, β-galactosidase staining of the AVN was much smaller (Figure 5A). Quantitative analyses of the stained AVN supported this notion (Figure 5B). RT-PCR analyses showed that, among several proteins potentially involved in regulation of HR, expression of Nkx2.5 is attenuated while that of HCN-1 is upregulated in Tg-i2m compared with Tg-WT mice (Table 6), similar to the pattern observed in Nkx2.5 KO mice, which also develop AV block (31).

At the cellular level, cardiac pacemaking is produced by the slow diastolic depolarization. Several ion channels contribute to pacemaker depolarization, including L-type Ca^{2+} channels (32, 33). To examine the cellular mechanisms causing bradycardia in Tg-i2m mice, we examined L-type Ca^{2+} channel currents (I_{Ca}) in atrial myocytes isolated from NTg and Tg-i2m mice. The Tg-i2m mice exhibited significantly smaller I_{Ca} amplitude compared with NTg mice. Peak inward I_{Ca} amplitude, normalized relative to cell capacitance (pA/pF), as a function of voltage was plotted (Figure 5C). The data demonstrated no significant difference in the current-voltage (i-V) relationships but showed a significant decrease in peak I_{Ca} density in Tg-i2m mouse myocytes compared with NTg mouse myocytes.

Table 2
Echocardiographic analyses of Tg-WT and Tg-i2m mice

	AT1-WT		AT1-i2m	
	NTg	Tg	NTg	Tg
n	8	8	11	10
Age (d)	309 ± 5	309 ± 2	302.9 ± 34.5	303.1 ± 39.1
DSEPWT (mm)	0.77 ± 0.03	0.75 ± 0.06	0.80 ± 0.03	0.80 ± 0.03
LVEDD (mm)	3.72 ± 0.07	4.54 ± 0.09[A]	3.83 ± 0.06	5.82 ± 0.17[B,C]
DPWT (mm)	0.74 ± 0.03	0.75 ± 0.07	0.74 ± 0.03	0.77 ± 0.02
LVESD (mm)	2.47 ± 0.05	3.06 ± 0.06[D]	2.50 ± 0.05	3.98 ± 0.15[B,C]
EF (%)	71.55 ± 0.51	68.13 ± 1.07[E]	72.09 ± 0.64	68.00 ± 1.26[E]
FS (%)	34.10 ± 0.33	31.66 ± 0.88[E]	34.71 ± 0.51	31.78 ± 0.91[E]
HR (bpm)	437 ± 22	301 ± 6[D]	437 ± 12	173 ± 15[B,C]

$^{A}P < 0.01$ and $^{B}P < 0.0001$ compared with corresponding NTg mice; $^{C}P < 0.01$ compared with Tg-WT mice; $^{D}P < 0.001$ and $^{E}P < 0.05$ compared with corresponding NTg mice. DSEPWT, diastolic septal wall thickness; DPWT, diastolic posterior wall thickness; EF, ejection fraction; FS, fractional shortening.

Table 3
Conscious HRs of newborn Tg-WT and Tg-i2m mice

	AT1-WT				AT1-i2m			
	NTg		Tg		NTg		Tg	
n	4	6	3	4	4	4	4	4
Age (d)	10.0 ± 0.0	21.2 ± 0.2	10.0 ± 0.0	21.3 ± 0.3	12.3 ± 0.8	23.5 ± 0.5	11.5 ± 0.9	23 ± 0.6
HR (bpm)	515 ± 43	753 ± 3	535 ± 18	420 ± 60[A]	584 ± 20	689 ± 66	566 ± 13	318 ± 4[B,C]

[A]$P < 0.0005$ and [B]$P < 0.005$ compared with corresponding age-matched NTg mice; [C]$P < 0.005$ compared with age-matched Tg-WT mice.

A lack of depolarization shift indicates that changes in Cav1.3 (αD-type channel) do not significantly contribute to the overall decrease in atrial I_{Ca} (34). I_{Ca} density in atrial myocytes from Tg-WT mice was not significantly different from that in NTg mouse myocytes (Figure 5C). Similarly, I_{Ca} density in ventricular myocytes isolated from Tg-WT mice (9.0 ± 0.4 *pA/pF*; $n = 24$) was not different from that in NTg mouse myocytes (8.2 ± 0.5 *pA/pF*; $n = 38$), while a significant decrease in I_{Ca} density (6.9 ± 0.4 *pA/pF*; $n = 31$, $P < 0.05$) was observed in Tg-i2m mouse myocytes. These data show that Tg-i2m mice have decreased Ca^{2+} entry during depolarization, which may contribute in part to bradycardia.

To understand the cellular mechanisms underlying the LV dysfunction in Tg-i2m mice, we examined isolated cell contractility. The amplitude of myocyte contraction (% cell shortening) did not differ between cardiac myocytes from NTg and Tg-WT mice while that in myocytes from Tg-i2m mice was significantly smaller (Figure 5D), indicating that cellular contractility is depressed in Tg-i2m mice. Taken together, these findings suggest that there may be LV systolic and diastolic dysfunction in the Tg-i2m mice although the results of echocardiographic studies (Table 2) and experiments on isolated cardiac myocytes (Figure 5D) display more modest/subtle alterations.

Tg-i2m mouse hearts have less fibrosis and apoptosis than Tg-WT mouse hearts. The level of interstitial fibrosis was increased in Tg-WT and Tg-i2m mice compared with corresponding NTg mice. Quantitative analyses indicated that the level of fibrosis in Tg-i2m mice was significantly less than that in Tg-WT mice (Figure 6, A and B). To evaluate the frequency of cardiac myocyte cell death in the myocardium, TUNEL staining was performed on cardiac sections from 10- to 12-month-old mice. Significantly more TUNEL-positive myocytes were observed in Tg-WT and Tg-i2m mice than in the corresponding NTg mice. The level of apoptosis was significantly smaller in Tg-i2m than in Tg-WT mice (Figure 6C) despite the fact that Tg-i2m mice have higher ventricular wall stress than Tg-WT mice.

Chronic Ang II infusion causes greater cardiac hypertrophy in Tg-i2m mice whereas acute Ang II administration increased HR only in Tg-WT mice. Continuous infusion of Ang II (200 ng/kg/min) for 2 weeks resulted in a significant increase in LVW/BW and LVW/TL in both Tg-WT and Tg-i2m mice, whereas a greater increase was observed in Tg-i2m mice (Figure 7A). Ang II infusion did not significantly affect blood pressure in either group of mice (Supplemental Figure 4). In contrast, intravenous bolus injection of Ang II (100 ng/kg) increased the HR in Tg-WT but not in Tg-i2m mice (Figure 7B). The lack of Ang II–induced HR response in Tg-i2m mice was unlikely to be due to general insensitivity because the HR response to isoproterenol, an agonist for the β-adrenergic receptor, was actually enhanced in Tg-i2m compared with Tg-WT mice (Supplemental Figure 5).

ERKs were more strongly activated but stayed in the cytoplasm while PKCε was not translocated to the particulate fraction in Tg-i2m mice. We have shown previously in CHO-K1 cells that binding of Ang II to AT1-i2m induces activation of ERKs, which fail to enter the nucleus (16). To compare the activity of ERKs in Tg-WT and Tg-i2m mice in the heart, immunoblotting using phospho-ERK antibod-

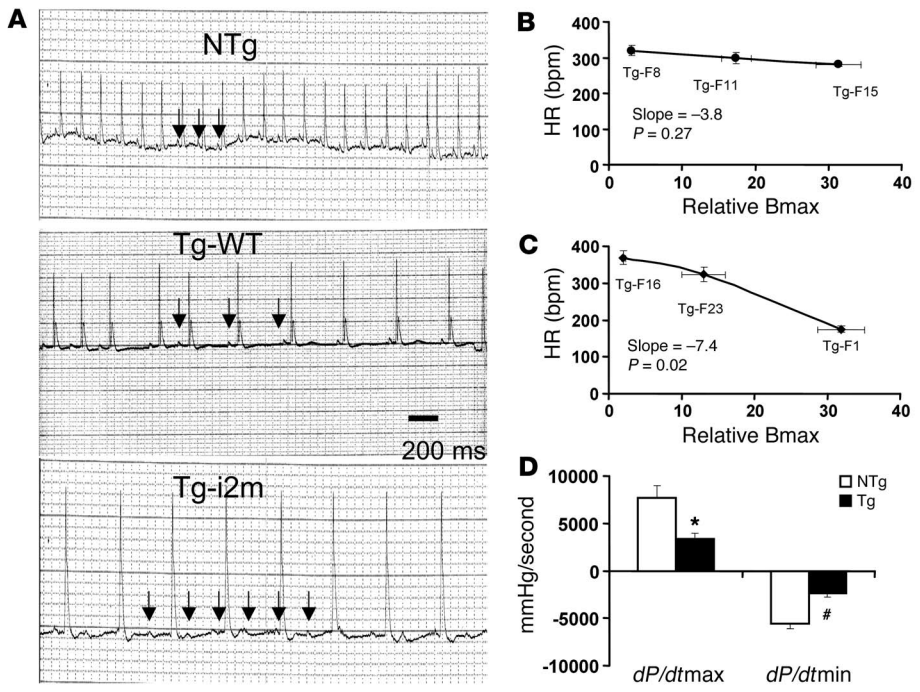

Figure 4
Bradycardia, AV block, and LV function. (**A**) Representative lead II ECG of NTg ($n = 10$), Tg-WT (line 15, $n = 10$), and Tg-i2m mice (line 1, $n = 10$). Arrows point to P wave. Marked bradycardia and complete AV block are typically seen in Tg-i2m mice while moderate bradycardia and second-degree AV block are seen in Tg-WT mice. (**B** and **C**) The relationship between HR and AT1 receptor expression level in Tg-WT in **B** (line 8, $n = 6$, line 11, $n = 4$, line 15, $n = 5$) and Tg-i2m mice in **C** (line 16, $n = 6$, line 23, $n = 4$, line 1, $n = 7$). There is a dose-dependent decrease in HR in Tg-i2m but not in Tg-WT mice. (**D**) LV *dP/dt* of Tg-i2m (line 1, $n = 4$) and littermate NTg mice ($n = 4$) when heart was paced at 500 bpm. *$P < 0.05$, #$P < 0.01$ vs. NTg mice.

Table 4
Measurements of ECG intervals of Tg-WT and Tg-i2m mice

	NTg	Tg-WT	Tg-i2m
HR (bpm)	488 ± 15	275 ± 17[A]	183 ± 11[A,B]
PR interval (ms)	34.9 ± 1.3	48.8 ± 2.3	N/A
QRS interval (ms)	15.3 ± 0.6	17.2 ± 0.6	38.8 ± 1.3[B,C]
QTc interval (ms)	53.1 ± 3.0	65.0 ± 3.9	58.9 ± 4.3

[A]$P < 0.0001$ compared with NTg mice; [B]$P < 0.001$ compared with Tg-WT mice; [C]$P < 0.01$ compared with NTg mice. PR interval, interval between P and R waves; QTc interval, corrected interval between Q wave and T wave.

ies was carried out. Both Tg-WT and Tg-i2m mice showed significantly increased phospho-ERKs/total ERKs ratios compared with corresponding NTg mice in whole cell lysates, with Tg-i2m mice exhibiting a higher level of phospho-ERKs than Tg-WT mice (Figure 8A). Interestingly, the amount of phospho-ERKs in the nuclear fraction, on the other hand, was significantly greater in Tg-WT mice than in either Tg-i2m or NTg mice (Figure 8B). These data suggest that ERKs activated in Tg-i2m mice failed to translocate into the nucleus. Immunostaining of neonatal rat cardiac myocytes showed that Ang II treatment induced nuclear accumulation of phospho-ERKs in cells overexpressing AT1-WT and cytoplasmic accumulation in those overexpressing AT1-i2m (Supplemental Figure 7). Tg-WT mouse hearts exhibited modest but significant activation of p46-JNK and p38-MAPK, which was not observed in Tg-i2m mouse hearts (Figure 8, C and D). In CHO-K1 cells, ERK activation by AT1-i2m is also accompanied by activation of Src (16). Tg-i2m mice showed a significantly elevated phospho-Src/total Src ratio compared with NTg mice, while Src was not activated in Tg-WT mice (Figure 8E).

Phosphoprotein enriched in astrocytes (PEA-15) plays an important role in mediating cytoplasmic sequestration of ERKs in NIH 3T3 cells (35). PEA-15 is phosphorylated by PKC and Ca^{2+}/calmodulin kinase (36). Tg-WT mice exhibited a higher phospho–PEA-15/total PEA-15 ratio than either NTg or Tg-i2m mice (Figure 8F), which potentially explains nuclear translocation of ERKs in Tg-WT but not in Tg-i2m mice.

To confirm that the $G_\alpha q$-dependent signaling is not stimulated in Tg-i2m mice, immunoblotting of PKCε was carried out. In Tg-WT mice, PKCε was translocated into the particulate fraction, as evidenced by an increase in particulate/cytosolic PKCε. However, this translocation of PKCε was not observed in Tg-i2m mice (Figure 8G). Redistribution of $G_\alpha q$ into the cytosol has been shown to be an indirect marker of $G_\alpha q$ activation (37) and was observed in Tg-WT but not in Tg-i2m mice (Figure 8H). These results are consistent with the notion that $G_\alpha q$-dependent signaling is not stimulated in Tg-i2m mice.

In order to confirm that signaling molecules have distinct subcellular localization in Tg-WT and Tg-i2m mice, immunohistochemical analyses were conducted on LV myocardial sections. In Tg-WT mouse hearts, more phospho-ERK positive nuclei were found compared with NTg and Tg-i2m mouse hearts. In contrast, increases in phospho-ERK staining were observed primarily in the cytoplasm of cardiac myocytes in Tg-i2m mice (Figure 8I). In addition, staining of PKCε is primarily found in the plasma membrane in Tg-WT but not in Tg-i2m hearts (Figure 8I). These results are consistent with those obtained by immunoblot analyses and further support the notion that the effector of $G_\alpha q$ signaling is not activated while ERKs are activated only in the cytoplasm of cardiac myocytes in Tg-i2m mice.

Discussion

Transgenic mice with cardiac-specific overexpression of AT1-i2m, which does not couple to $G_\alpha q$ or $G_\alpha i$, exhibited greater cardiac hypertrophy, cardiac dysfunction, and bradycardia but less apoptosis and fibrosis than those overexpressing AT1-WT (Supplemental Table 3). AT1 receptors have traditionally been thought to mediate cellular functions through interaction with heterotrimeric G proteins, predominantly $G_\alpha q$ and $G_\alpha i$. However, increasing lines of evidence suggest that GPCRs can initiate signaling mechanisms through unconventional mechanisms, including heterotrimeric G protein–independent mechanisms (38–41). Our results suggest that such mechanisms potentially mediate pathologically relevant cardiac phenotypes initiated by the AT1 receptor in the heart in vivo.

Our previous in vitro study showed that AT1-i2m activates, independently of $G_\alpha q/G_\alpha i$ protein, the Src/Ras/ERK pathway without nuclear translocation of ERKs in CHO-K1 cells (16). AT1-i2m expressed in cultured cardiac myocytes also exhibited insensitivity to GTPγS-induced displacement of ligand binding and cytoplasmic accumulation of phospho-ERK in response to Ang II, similar to AT1-i2m in CHO-K1 cells (16). AT1-i2m expressed in the mouse heart also exhibited clear differences in its effect upon downstream signaling compared with AT1-WT. For example, translocation of PKCε to the particulate fraction as well as PEA-15 Ser 116 phosphorylation observed in Tg-WT mice were missing in Tg-i2m mice. Accumulation of phospho-ERKs in the cytoplasm but not in the nucleus was observed in cardiac myocytes from Tg-i2m mice, a finding similar to that obtained in CHO-K1 cells (16). Furthermore, redistribution of $G_\alpha q$ into the cytosolic fraction, another indicator of $G_\alpha q$ activation (37), was observed in myocytes from Tg-WT but not from Tg-i2m mice. Although a potential involvement of other heterotrimeric G proteins, such as $G_\alpha 12/G_\alpha 13$, in mediating the cardiac phenotype of Tg-i2m mice cannot be formally excluded, these results are consistent with the notion that cell-signaling mechanisms dependent upon $G_\alpha q/G_\alpha i$, the major heterotrimeric G proteins in the heart, are not stimulated whereas the $G_\alpha q/G_\alpha i$-independent signaling mechanism is activated in cardiac myocytes from Tg-i2m mice.

Table 5
Hemodynamic measurements of Tg-WT and Tg-i2m mice

	AT1-WT		AT1-i2m	
	NTg	Tg	NTg	Tg
n	8	5	7	7
LVSP (mmHg)	89 ± 5	83 ± 5	90 ± 6.6	83 ± 1.9
LVEDP (mmHg)	6.5 ± 1.2	5.2 ± 1.2	4.5 ± 0.3	12.9 ± 2.3[A,B]
+*dP/dt* (mmHg/s)	7875 ± 812	5000 ± 506[C]	7171 ± 371	3828 ± 515[A,B]
−*dP/dt* (mmHg/s)	6250 ± 550	3780 ± 358[A]	6400 ± 373	3129 ± 394[B,D]
MAP (mmHg)	69.1 ± 5.4	58.1 ± 7.5	66.9 ± 5.0	57.6 ± 3.4
HR (bpm)	445 ± 23	273 ± 7[D]	429 ± 24	175 ± 9[B,E]

[A]$P < 0.01$ compared with corresponding NTg mice; [B]$P < 0.05$ compared with Tg-WT mice; [C]$P < 0.05$, [D]$P < 0.001$, and [E]$P < 0.0001$ compared with corresponding NTg mice. LVEDP, LV end-diastolic pressure; LVSP, LV systolic pressure.

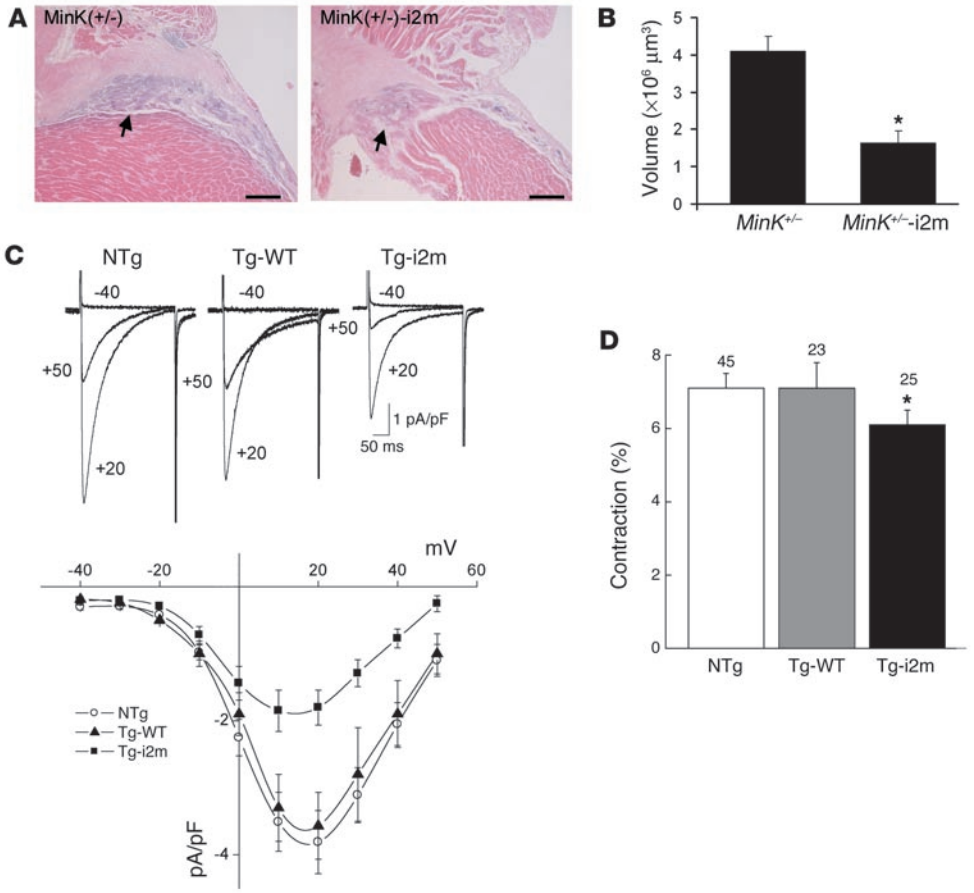

Figure 5

Morphology of AV node, calcium currents, and contraction. (**A**) Images obtained from β-gal–stained hearts to show AVN. Arrows point to AVN. A significantly smaller AVN was seen in *MinK*$^{+/-}$ Tg-i2m mouse hearts compared with *MinK*$^{+/-}$ hearts. Scale bars: 10 μm. (**B**) The estimated volume of AVN. Since the thickness of the serial section was 6 μm, if AVN can be observed in n sections and the area of AVN in the section k is S_k μm^2, the volume of AVN (μm^3) is roughly estimated as $6 \times (S_1+S_2+S_3+ \ldots +S_n)$. *$P < 0.05$ vs. *MinK*$^{+/-}$. (**C**) I_{Ca} of atrial myocytes from NTg, Tg-WT, and Tg-i2m mice. I_{Ca} density, calculated as peak inward I_{Ca} amplitude normalized to cell capacitance (*pA/pF*), is shown. Tg-i2m mice exhibited significantly smaller I_{Ca} amplitude compared with NTg and Tg-WT mice. There is a significant decrease in I_{Ca} density in myocytes from Tg-i2m mice compared with myocytes from NTg or Tg-WT mice. Data points are mean I_{Ca} density ± SEM in atrial myocytes of Tg-i2m ($n = 22$), Tg-WT ($n = 24$), and NTg ($n = 50$) mice from 4 Tg-i2m (line 1), 6 Tg-WT (line 15), and 6 NTg mouse littermates, respectively. (**D**) Myocyte contraction recorded in Tg-WT and Tg-i2m mouse myocytes. Data are means ± SEM. Numbers correspond to total number of cells measured. *$P < 0.05$ vs. NTg mice. Data points are from 8 NTg, 7 Tg-WT, and 9 Tg-i2m mice. The difference between NTg and Tg-i2m mice was also significant ($P < 0.05$) when the statistical analysis was conducted based upon the number of mice (NTg, 7.5% ± 0.2%; Tg-WT, 7.0% ± 1.1%; Tg-i2m 5.7% ± 0.5%).

The fact that Tg-i2m mice dose-dependently developed hypertrophy indicates that AT1 receptors can initiate hypertrophy through $G_\alpha q$- or $G_\alpha i$-independent mechanisms. Although cardiac dysfunction and/or bradycardia could induce hypertrophy secondarily, we believe that these alone may not explain the robust hypertrophy in Tg-i2m mice because hypertrophy has not necessarily been observed in other transgenic mouse models of bradycardia, AV conduction abnormality, and/or cardiac dysfunction (42–44). Losartan partially reversed cardiac hypertrophy without affecting bradycardia. Furthermore, expression of AT1-i2m in cultured myocytes also enhanced Ang II–induced hypertrophy at the single-cell level, indicating that AT1-i2m has direct hypertrophic effects. Interestingly, in vitro dose-response experiments showed that a higher degree of hypertrophy was induced at lower concentrations of Ang II in myocytes expressing AT1-i2m compared with those expressing AT1-WT, suggesting that AT1-i2m is a more sensitive stimulator of cardiac hypertrophy. We have previously shown that ligand-dependent down-regulation of AT1-i2m is partially impaired, possibly due to the lack of feedback from the $G_\alpha q$ pathway (45), which may contribute to the enhanced hypertrophic response in Tg-i2m mice.

Recent evidence suggests that GPCRs can form either homo- or hetero-oligomers (46). At present, the involvement of oligomerization between exogenous AT1-i2m and endogenous AT1 receptors or other unknown GPCRs in mediating cardiac hypertrophy cannot be formally excluded (15, 47). However, we believe that this possibility is remote because oligomerization with other $G_\alpha q$- or $G_\alpha i$-coupled receptors could have made ligand binding of AT1-i2m GTPγS-sensitive. Such a hetero-oligomerization property could have been shared with AT1-WT, and if so, AT1-WT should have shown a similar dose-dependent effect upon hypertrophy as AT1-i2m. If AT1-i2m works as a dominant receptor over endogenous AT1 receptors, cardiac phenotype in Tg-i2m mice could be in part caused by suppression of the endogenous AT1 receptors. We believe that this is unlikely because neither AT1 receptor antagonist treatment nor AT1-receptor knockout mice exhibit a cardiac phenotype similar to Tg-i2m mice, such as hypertrophy and bradycardia (48).

At present, we do not know the downstream signaling mechanism mediating greater hypertrophy in Tg-i2m mice. Thus far, we have shown that activation of total ERK and Src is higher in Tg-i2m than in Tg-WT mice. On the other hand, nuclear accumulation of ERK and activation of PKCε are observed in Tg-WT but not in Tg-i2m mice. Cardiac-specific expression of an activated form of MEK1 induces well-compensated hypertrophy in Tg mice (27), which is similar to the compensated hypertrophy seen in Tg-i2m mice, in which less apoptosis and fibrosis were observed compared with Tg-WT mice despite a higher degree of hypertrophy. On the other hand, members of the Src family of tyrosine kinases are likely to have diverse roles in mediating cardiac hypertrophy (49–51). In

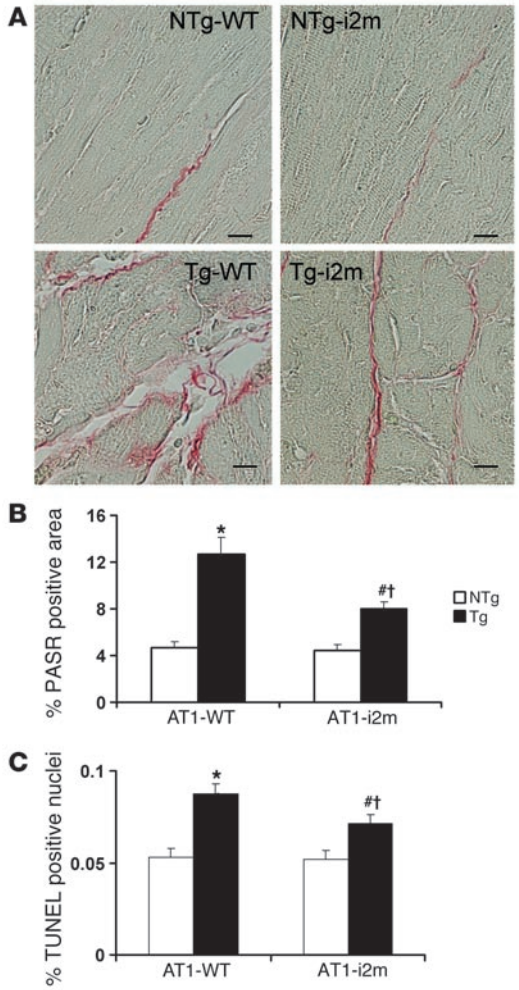

Figure 6
Myocardial fibrosis and apoptosis. (**A**) Picric acid Sirius red (PASR) staining of heart sections obtained from Tg-WT (line 15, $n = 5$) and Tg-i2m (line 1, $n = 7$) mice. Significantly more fibrosis is seen in both Tg-WT and Tg-i2m mice than in their NTg littermates ($n = 4$ and $n = 6$, respectively), but Tg-i2m mice had significantly less fibrosis than Tg-WT mice. Scale bars: 1 μm. (**B**) Morphometry of myocardial fibrosis. (**C**) Morphometry of TUNEL staining of myocardial sections from NTg ($n = 4$ and $n = 6$ for AT1-WT and AT1-i2m, respectively), Tg-WT (line 15, $n = 5$), and Tg-i2m mice (line 1, $n = 7$). Tg-i2m mice had significantly fewer TUNEL-positive myocytes than Tg-WT mice. $^{*}P < 0.01$, $^{\#}P < 0.05$ compared with NTg mice; $^{\dagger}P < 0.05$ compared with Tg-WT mice.

vitro experiments using cultured cardiac myocytes indicated that chemical inhibitors of MEK1 and Src significantly attenuated Ang II–induced hypertrophy in AT1-i2m transduced cardiac myocytes (Supplemental Results and Supplemental Figure 8). Whether or not increased activation of Src or ERK is critical for the development of hypertrophy in Tg-i2m mice in vivo remains to be elucidated.

We have previously shown that overexpression of AT1-i2m fails to induce Ang II–induced cell proliferation in CHO-K1 cells (16). Thus, AT1-i2m seems to differentially affect proliferation and hypertrophy. Alternatively, the effect of AT1-i2m upon cell-growth responses and the underlying signaling mechanisms may differ in a cell type–dependent manner.

Our results are consistent with a previous report showing that cardiac-specific overexpression of the AT1 receptor causes bradycardia in transgenic mice (52). Our results are unique, however, in that Tg-i2m mice developed more severe bradycardia and heart block than Tg-WT mice. Given that the AT1 receptor is expressed in the cardiac conduction system (53, 54) and that Ang II decreases junctional conductance between cardiac myocardial cells (55), the AT1 receptor seems to affect either development or function of the cardiac conduction system. For example, in Tg-WT mice, the AT1 receptor may couple to $G_{\alpha}i$, which in turn mediates inhibition of potassium channels, leading to bradycardia (56). However, the fact that more severe bradycardia is induced in Tg-i2m mice suggests that the $G_{\alpha}i$ signaling may not be the sole mechanism. Interestingly, Tg-i2m mice exhibited a poorly developed AVN, suggesting that the development of the conduction system may be perturbed by dysregulated signals from AT1-i2m. Tg-i2m mice also exhibited downregulation of Nkx2.5 and marked upregulation of HCN-1, a finding similar to ventricular-specific Nkx2.5 KO mice, which show progressive AV block (31). In addition, atrial myocytes prepared from Tg-i2m mice exhibited smaller I_{Ca}, known to be involved in regulation of HR. The fact that complete AV block was not rescued by losartan treatment suggests that persistent defects, such as anatomical ones, are involved at least in part in the mechanism of AV block. Elucidation of the specific targets of AT1-i2m would reveal important mechanisms regulating AV conduction and HRs.

Tg-i2m mice exhibited more severe cardiac dysfunction than Tg-WT mice. The cardiac dysfunction in Tg-i2m mice may not be directly related to the increases in apoptosis and fibrosis because Tg-i2m mice showed less apoptosis and fibrosis than Tg-WT mice. In fact, ventricular myocytes isolated from Tg-i2m mice showed reduced contractility at the single-cell level. Ca^{2+} influx through voltage-gated Ca^{2+} channels is an important trigger for Ca^{2+}-induced Ca^{2+} release from the sarcoplasmic reticulum. Thus, a decrease in I_{Ca} may play an important role in mediating decreased contractility in Tg-i2m mice. Since the decrease in I_{Ca} was not significant in Tg-WT mice, it may be mediated by $G_{\alpha}q$- or $G_{\alpha}i$-independent mechanisms. Although external application of Ang II could enhance I_{Ca} in ventricular myocytes isolated from some species, the effect seems to differ depending upon experimental conditions (57, 58). Interestingly, I_{Ca} in ventricular myocytes was not directly modulated by Ang II (Supplemental Results and Supplemental Figure 6). Thus, decreases in I_{Ca} are mediated by long-term activation of $G_{\alpha}q$- or $G_{\alpha}i$-independent mechanisms rather than ligand-dependent short-term modulation in Tg-i2m mice.

The present study showed that the percentage of apoptotic myocytes was significantly greater in Tg-WT than in Tg-i2m mice. These data indicate that AT1 receptor–induced myocardial cell death is more strongly mediated by a $G_{\alpha}q$- or $G_{\alpha}i$-dependent mechanism. Our result is consistent with previous observations that enhanced $G_{\alpha}q$ signaling is sufficient to induce cardiac myocyte apoptosis (59, 60) and thus could be detrimental. The $G_{\alpha}q/G_{\alpha}i$-independent signaling mechanism activated in Tg-i2m mice causes less myocardial apoptosis and therefore may be less detrimental.

Activated ERKs are found primarily in the nucleus in Tg-WT mouse cardiac myocytes while they are primarily in the cytoplasm in Tg-i2m mouse myocytes. Activated ERKs can be localized to the cytoplasm by cytoplasmic anchors, such as PEA-15 (35, 61). PEA-15 has been reported to constitutively bind both ERKs and ribosomal

Table 6
Gene transcripts measured by RT-qPCR

mRNA		Tg-WT mice (fold change) ($n = 5$)	Tg-i2m mice (fold change) ($n = 7$)
Cx 37	Gap junction	0.16 ± 0.02	0.85 ± 0.07
Cx 40	Gap junction	0.95 ± 0.62	1.03 ± 0.11
Cx 43	Gap junction	0.77 ± 0.44	1.46 ± 0.46
SCN5a	Sodium channel	0.77 ± 0.13	0.91 ± 0.21
Nkx2.5	Transcription factor	0.86 ± 0.15	0.58 ± 0.12[A]
HCN-1	Hyperpolarization-activated cyclic nucleotide-gated channel	0.90 ± 0.37	11.0 ± 2.9[A]
KCNE-1	Minimal potassium channel	0.40 ± 0.25	1.17 ± 0.58
SLN	Inhibitor of SERCA	0.85 ± 0.61	0.16 ± 0.1

[A]$P < 0.05$ compared with NTg mice.

protein S6 kinase II (RSK2), thereby retaining both in the cytoplasm (35, 61). PEA-15 is phosphorylated at serine 104 by PKC and at serine 116 by Ca^{2+}/calmodulin kinase II, both of which are activated by $G_{\alpha}q$ signaling (36). We have shown here that there is more phospho(S^{116})–PEA-15 in Tg-WT mice cardiac myocytes. Whether or not phosphorylation of PEA-15 by $G_{\alpha}q$ signaling regulates nuclear localization of ERKs remains to be elucidated. However, our results clearly suggest that ERKs activated by distinct upstream signaling mechanisms are subjected to distinct subcellular localizations in vivo.

In conclusion, the data presented here show that the AT1 receptor mediates downstream signaling mechanisms through $G_{\alpha}q$/$G_{\alpha}i$-dependent and -independent mechanisms, which in turn modulate hypertrophy with distinct phenotypes. This suggests the possibility of a novel strategy for the treatment of heart disease by modulating these unconventional signaling mechanisms initiated by the AT1 receptor.

Methods

Primary culture of neonatal rat ventricular myocytes. Primary cultures of ventricular cardiac myocytes were prepared from 1-day-old Crl: (WI) BR-Wistar rats (Charles River Laboratories) as previously described (62). A cardiac myocyte–rich fraction was obtained by centrifugation through a discontinuous Percoll gradient as described (63). All protocols concerning animal use were approved by the Institutional Animal Care and Use Committee at the University of Medicine and Dentistry of New Jersey.

Construction of the adenoviral vectors. Recombinant adenovirus was constructed using an Adeno-X adenovirus construction kit (BD Biosciences — Clontech). We made replication-defective human adenovirus type 5 (devoid of E1 and E3) harboring AT1-WT (Ad–AT1-WT) and AT1-i2m (Ad–AT1-i2m).

Receptor-binding assays. Radioligand-binding assays were performed as described previously (16). Myocytes were lysed and hearts homogenized with CHAPS buffer containing 150 mmol/l NaCl, 40 mmol/l Tris pH 7.5, 1% Triton X-100, 0.1% CHAPS, 10% glycerol, 2 mmol/l EDTA, 10 mmol/l sodium pyrophosphate, 1 mmol/l Na_3VO_4, 10 mmol/l NaF, 0.5 mmol/l AEBSF, 0.5 μg/ml aprotinin, and 0.5 μg/ml leupeptin. The cell lysates were incubated with 0.1 nmol/l [^{125}I]-Sar^1-Ile^8-Ang II in 50 mmol/l Tris (pH 7.5) buffer containing 200 mmol/l NaCl, 10 mmol/l $MgCl_2$, 1 mmol/l EDTA, 0.1% bovine serum albumin, and 0.01% trypsin inhibitor at room temperature for 60 minutes in the presence of varying concentrations of GTPγS. Bound radioligand was separated from free ligand and the radioactivity counted. Specific AT1-receptor binding was determined by the addition of losartan (10 μM). Binding data were analyzed using Prism 3.0 (GraphPad Software).

Transgenic mice. Tg-WT mice and Tg-i2m mice were generated on an FVB background using the α-myosin heavy chain promoter (courtesy of J. Robbins, University of Cincinnati, Cincinnati, Ohio, USA) to achieve cardiac-specific expression. Comparison of cardiac phenotype in Tg-WT mice among ours and those generated by other investigators (52, 64) is summarized in Supplemental Results and Supplemental Table 4.

Protein content. Total protein content of cultured cardiac myocytes was determined as described previously (63).

Quantitative RT-PCR. Total RNA was prepared using the RNeasy fibrous tissue kit (QIAGEN), and then first-strand cDNA was synthesized using the ThermoScript RT-PCR system (Invitrogen Corp.). Real-time PCR was then carried out on a DNA Engine Opticon 2 system (MJ Research Inc.) using the DyNAmo HS SYBR Green qPCR kit (Finnzymes). The specific oligonucleotide primers used in this study are described in Supplemental Methods.

Echocardiography. Mice were anesthetized using 12 μl/g BW of 2.5% avertin (Sigma-Aldrich), and echocardiography was performed using ultrasonography (Acuson Sequoia C256; Siemens Medical Solutions) as previously described (65). A 13-MHz linear ultrasound transducer was used. We took 2D-guided motion mode measurements of LV internal diameter from more than 3 beats and averaged the measurements. LVEDD was measured at the time of the apparent maximal LVEDD while LVESD was measured at the time of the most anterior systolic excursion of the posterior wall.

Hemodynamic measurements, intracardiac pacing, and ECG measurements. Mice were anesthetized as described above, and a 1.4-French (Millar Instruments Inc.) catheter-tip micromanometer catheter was inserted through the right carotid artery into the aorta and then into the LV where pressures and LV *dP/dt* were recorded. In order to pace the heart, a 1.1 French Millar EPR-800

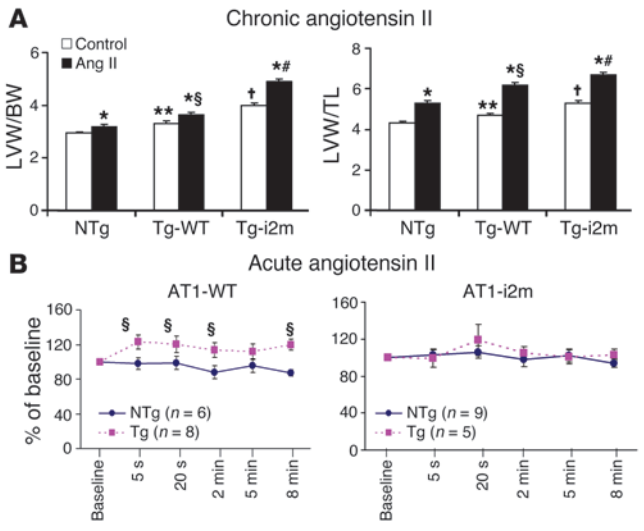

Figure 7
Changes in hypertrophy and HR in response to Ang II. (**A**) Hypertrophic response to 2 weeks Ang II infusion (200 ng/kg/min). *$P < 0.01$ vs. corresponding control. §$P < 0.05$ vs. control Ang II; #$P < 0.05$ vs. Tg-WT Ang II; **$P < 0.05$ vs. NTg control; †$P < 0.01$ Tg-WT control. $n = 5$ for all groups. (**B**) HR response to acute intravenous injection of Ang II (100 ng/kg). §$P < 0.05$ Tg-WT vs. Tg-i2m, Tg-WT mice exhibited increases in the atrial (P wave) rate in response to Ang II while Tg-i2m mice showed complete AV block and ventricular rates that did not respond to Ang II. $n = 6$ for NTg-WT; $n = 8$ for Tg-WT; $n = 9$ for NTg-i2m; and $n = 5$ for Tg-i2m mice.

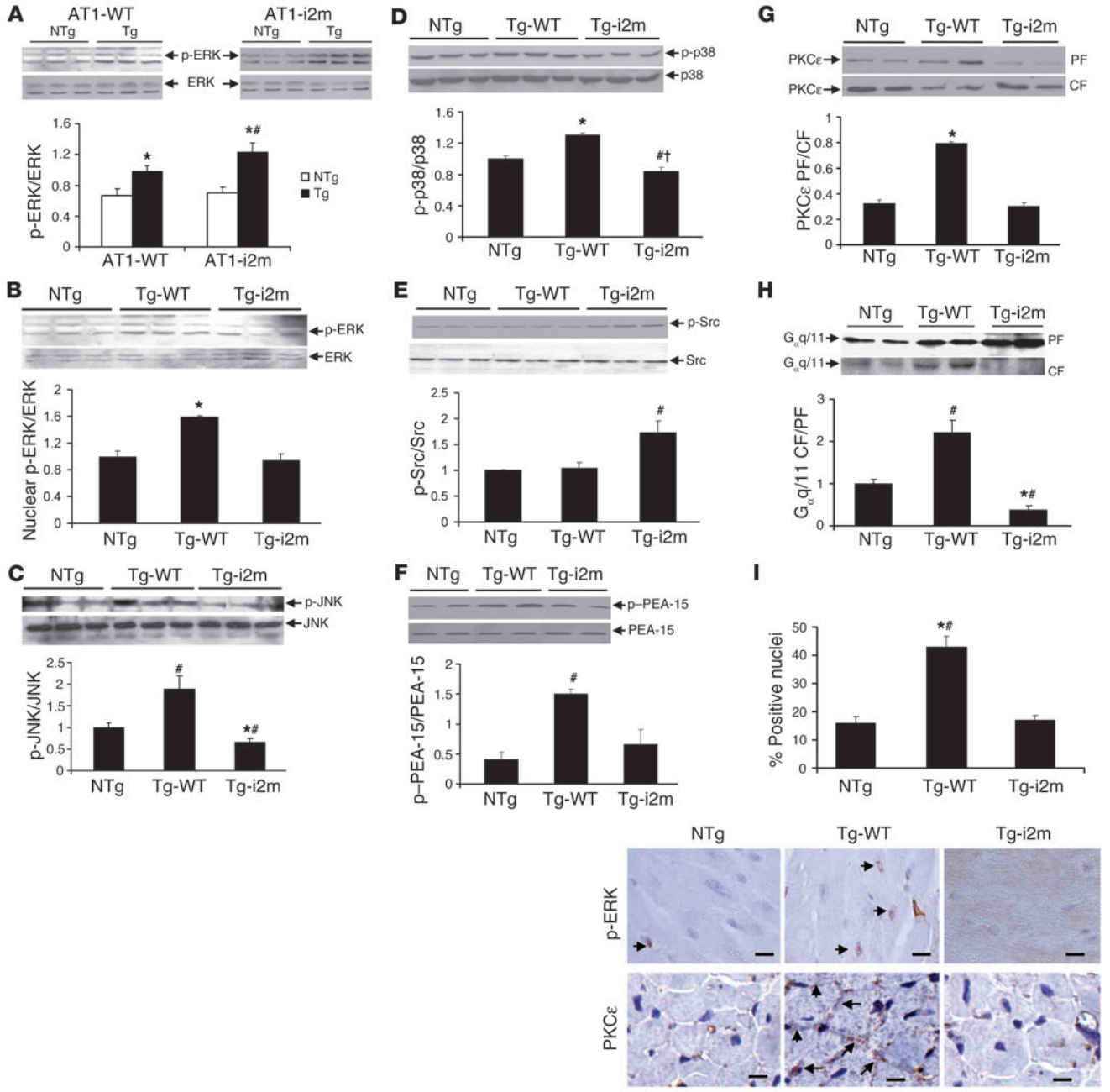

Figure 8

Cell-signaling mechanisms in Tg-WT and TG-i2m mice. (**A**) Immunoblotting of phospho-ERK (p-ERK) and total ERK in the cytosolic fraction. *$P < 0.01$ vs. NTg; #$P < 0.05$ vs. AT1-WT. (**B**) Immunoblotting of p-ERK in the nuclear fraction. *$P < 0.01$ vs. NTg. (**C**) Immunoblotting of p-JNK and total JNK. #$P < 0.05$ vs. NTg; *$P < 0.01$ vs. Tg-WT. (**D**) Immunoblotting of p-p38 and total p38. *$P < 0.01$, #$P < 0.05$ vs. NTg; †$P < 0.001$ vs. Tg-WT. (**E**) Immunoblotting of p-Src and total Src in the particulate fraction. #$P < 0.05$ vs. NTg. (**F**) Immunoblotting of phospho–PEA-15 and total PEA-15 in the cytosolic fraction. #$P < 0.05$ vs. NTg. Experiments were conducted 3 times each for **A**–**F**. (**G**) Immunoblotting of PKCε in the particulate fraction (PF) and cytosolic fraction (CF) of Tg-WT and Tg-i2m mice. *$P < 0.01$ vs. NTg. (**H**) Immunoblotting of $G_\alpha q/11$ in PF and CF. Significantly more $G_\alpha q/11$ was translocated to the CF in Tg-WT than in Tg-i2m or NTg mice. #$P < 0.05$ vs. NTg. *$P < 0.01$ vs. Tg-WT. (**I**) Immunohistochemistry of p-ERK and PKCε. Arrows in upper panels indicate positive p-ERK–stained nuclei. Arrows in lower panels indicate membrane localization of PKCε. Scale bars: 1 μm. Bar graph shows quantitative analysis of nuclear p-ERK staining where the percentage ratio of p-ERK–positive nuclei is shown. Over 500 nuclei were counted per experiment. #$P < 0.05$ vs. NTg; *$P < 0.01$ vs. Tg-i2m. Experiments were conducted 3 times each for **G**–**I**.

ultraminiature catheter was introduced into the right ventricle through the left jugular vein. A body-surface ECG (leads I, II, and III) was recorded using 25-gauge subcutaneous electrodes while mice were under anesthesia. ECGs from neonatal mice were obtained while the mice were conscious and gently held.

Electrophysiological measurements. LV and atrial myocytes were enzymatically isolated and studied using whole-cell patch-clamp techniques (66). Cell capacitance was measured using voltage ramps of 0.8 V/s from a holding potential of –50 mV. I_{Ca} were recorded using a K^+- and Na^+-free

external solution (to isolate Ca^{2+} currents from other membrane currents and Na^+/Ca^{2+} exchanger) containing 2 mmol/l $CaCl_2$, 1 mmol/l $MgCl_2$, 135 mmol/l TEA-Cl, 5 mmol/l 4-aminopyridine, 10 mmol/l glucose, and 10 mmol/l HEPES (pH 7.3). The pipette solution contained 100 mmol/l Cs-aspartate, 20 mmol/l CsCl, 1 mmol/l $MgCl_2$, 2 mmol/l MgATP, 0.5 mmol/l GTP, 5 mmol/l EGTA, and 5 mmol/l HEPES (pH 7.3). Myocyte contraction was measured as previously described (67). Briefly, isolated LV myocytes were perfused with Tyrode solution composed of 135 mmol/l NaCl, 1.0 mmol/l $CaCl_2$, 1 mmol/l $MgCl_2$, 5.4 mmol/l KCl, 10 mmol/l glucose, and 5 mmol/l HEPES (pH 7.3) at 32°C and field stimulated at 1.0 Hz. Myocyte contraction was measured using a video motion edge detector.

MinK mice and staining for β-galactosidase activity. Generation of $MinK^{+/-}$ mice has been described (30). $MinK^{+/-}$ mice and Tg-i2m mice were crossed, and all experiments were conducted using $MinK^{+/-}$ mice with or without AT1-i2m transgene at F1 generation. Tg-i2m mice generated in $MinK^{+/-}$ background showed a phenotype similar to that of conventional Tg-i2m mice (Supplemental Table 5). The method of whole-heart β-galactosidase staining has been described (30).

Histological analysis and immunohistochemistry. Histological analyses of the heart sections were conducted as described previously (66). Heart specimens were fixed with 10% neutral buffered formalin, embedded in paraffin, and sectioned at 6-μm thickness. Interstitial fibrosis was evaluated by picric acid Sirius red staining. The positively stained (red) fibrotic area was measured and expressed as a percentage of total area. AVN was evaluated in 4-chamber view whole-heart sections stained with H&E and trichrome. Immunohistochemistry was carried out on cardiac tissue sections using anti–phospho-ERK antibodies (Cell Signaling Technology) and anti-PKCε antibodies (Upstate) as primary antibodies. Methods of immunostaining for cultured cells are described in Supplemental Methods.

Evaluation of apoptosis in tissue sections. DNA fragmentation was detected in situ using TUNEL, as described (65). In brief, deparaffinized sections were incubated with proteinase K, and DNA fragments were labeled with fluorescein-conjugated dUTP using TdT (Roche Diagnostics Corp.). The total number of nuclei was determined by manual counting of DAPI-stained nuclei in 6 fields of each section using the ×40 objective, and the number of TUNEL-positive nuclei was counted in the entire section. Limiting counting of total nuclei and the TUNEL-positive nuclei to areas with a true cross section of myocytes made it possible to selectively count only those nuclei that clearly were within myocytes.

Continuous infusion of Ang II. Continuous infusion of Ang II or control vehicle delivery was conducted using a min-osmotic pump (model 2002, ALZA). Ang II was prepared at a concentration calculated to deliver an average of 200 ng/kg/min during a 14-day infusion period. Control mice received pumps filled with 0.9% sodium chloride.

Immunoblot analysis. Cardiac tissue homogenates were made in the CHAPS buffer (Sigma-Aldrich). We used anti-phosphospecific and corresponding non-phosphospecific antibodies against Src (Tyr^{416}), PEA-15 (Ser^{116}), and ERK1/2 (Thr^{202}/Tyr^{204}) (Cell Signaling Technology) as primary antibodies. To detect PKCε translocation and the subcellular localization of phospho-ERK1/2, cardiac myocyte lysates, cardiac tissue homogenates, and nuclear, cytosolic, and particulate fractions were prepared as previously described (68) with mild modification. In brief, heart tissue was homogenized in a sample buffer containing 20 mmol/l Tris-HCl , 10 mmol/l EGTA, 5 mmol/l EDTA, 10 mmol/l benzamidine, 0.3% β-mercaptoethanol, 10 μg/ml aprotinin, 10 μg/ml leupeptin, and 50 μg/ml PMSF. The homogenate was loaded onto a sucrose gradient containing 2 ml of 1 mol/l sucrose in sample buffer and centrifuged at 1,600 *g* for 10 minutes. The pellet was resuspended in sample buffer containing 0.5% NP-40, 0.1% deoxycholate, and 0.1% Brij 35, then centrifuged at 9,300 *g* for 5 minutes after a 60-minute incubation on ice. The supernatant of the second centrifugation was the nuclear fraction. The supernatant of the first centrifugation was loaded onto another 1 mol/l sucrose gradient and centrifuged at 100,000 *g* for 60 min. The supernatant of the ultracentrifugation was the cytosolic fraction. The pellet of the ultracentrifugation was resuspended in the sample buffer, incubated on ice for 60 minutes, and centrifuged at 9,300 *g* for 5 minutes. The supernatant of the last centrifugation was the particulate fraction.

Statistics. Data are reported as mean ± SEM. Statistical analyses between groups were done by 1-way ANOVA, and when *P* values were significant, differences among group means were evaluated using *t* test with Bonferroni's correction. A *P* value of less than 0.05 was considered significant.

Acknowledgments

We thank Daniela Zablocki for critical reading of the manuscript. This work was supported by U.S. Public Health Service grants HL33107, HL59139, HL67724, HL67727, HL69020, and HL73048 and by American Heart Association grant 0340123N. Peiyong Zhai is supported by NIH training grant 1T32HL69752.

Note: A supplemental reference list is available online with this article.

Received for publication April 13, 2005, and accepted in revised form August 30, 2005.

Address correspondence to: Junichi Sadoshima, Cardiovascular Research Institute, University of Medicine and Dentistry of New Jersey, New Jersey Medical School, 185 South Orange Avenue, MSB G609, Newark, New Jersey 07103, USA. Phone: (973) 972-8619; Fax: (973) 972-8919; E-mail: sadoshju@umdnj.edu.

1. Nicholls, M.G., Robertson, J.I., and Inagami, T. 2001. The renin-angiotensin system in the twenty-first century. *Blood Press.* **10**:327–343.
2. Baker, K.M., Booz, G.W., and Dostal, D.E. 1992. Cardiac actions of angiotensin II: role of an intracardiac renin-angiotensin system. *Annu. Rev. Physiol.* **54**:227–241.
3. Pfeffer, J.M., Fischer, T.A., and Pfeffer, M.A. 1995. Angiotensin-converting enzyme inhibition and ventricular remodeling after myocardial infarction. *Annu. Rev. Physiol.* **57**:805–826.
4. Sadoshima, J., and Izumo, S. 1997. The cellular and molecular response of cardiac myocytes to mechanical stress. *Annu. Rev. Physiol.* **59**:551–571.
5. Dostal, D.E., Rothblum, K.N., Chernin, M.I., Cooper, G.R., and Baker, K.M. 1992. Intracardiac detection of angiotensinogen and renin: a localized renin-angiotensin system in neonatal rat heart. *Am. J. Physiol.* **263**:C838–C850.
6. Sadoshima, J., Xu, Y., Slayter, H.S., and Izumo, S. 1993. Autocrine release of angiotensin II mediates stretch-induced hypertrophy of cardiac myocytes in vitro. *Cell.* **75**:977–984.
7. Guo, D.F., Sun, Y.L., Hamet, P., and Inagami, T. 2001. The angiotensin II type 1 receptor and receptor-associated proteins. *Cell Res.* **11**:165–180.
8. Griendling, K.K., Lassegue, B., Murphy, T.J., and Alexander, R.W. 1994. Angiotensin II receptor pharmacology. *Adv. Pharmacol.* **28**:269–306.
9. Shirai, H., Takahashi, K., Katada, T., and Inagami, T. 1995. Mapping of G protein coupling sites of the angiotensin II type 1 receptor. *Hypertension.* **25**:726–730.
10. Doan, T.N., Ali, M.S., and Bernstein, K.E. 2001. Tyrosine kinase activation by the angiotensin II receptor in the absence of calcium signaling. *J. Biol. Chem.* **276**:20954–20958.
11. Tohgo, A., Pierce, K.L., Choy, E.W., Lefkowitz, R.J., and Luttrell, L.M. 2002. beta-Arrestin scaffolding of the ERK cascade enhances cytosolic ERK activity but inhibits ERK-mediated transcription following angiotensin AT1a receptor stimulation. *J. Biol. Chem.* **277**:9429–9436.
12. Holloway, A.C., et al. 2002. Side-chain substitutions within angiotensin II reveal different requirements for signaling, internalization, and phosphorylation of type 1A angiotensin receptors. *Mol. Pharmacol.* **61**:768–777.
13. Hines, J., Fluharty, S.J., and Yee, D.K. 2003. Structural determinants for the activation mechanism of the angiotensin II type 1 receptor differ for phosphoinositide hydrolysis and mitogen-activated protein kinase pathways. *Biochem. Pharmacol.* **66**:251–262.

14. Ahn, S., Wei, H., Garrison, T.R., and Lefkowitz, R.J. 2004. Reciprocal regulation of angiotensin receptor-activated extracellular signal-regulated kinases by beta-arrestins 1 and 2. *J. Biol. Chem.* **279**:7807–7811.
15. Hansen, J.L., Theilade, J., Haunso, S., and Sheikh, S.P. 2004. Oligomerization of wild type and non-functional mutant angiotensin II type I receptors inhibits galphaq protein signaling but not ERK activation. *J. Biol. Chem.* **279**:24108–24115.
16. Seta, K., Nanamori, M., Modrall, J.G., Neubig, R.R., and Sadoshima, J. 2002. AT1 receptor mutant lacking heterotrimeric G protein coupling activates the Src-Ras-ERK pathway without nuclear translocation of ERKs. *J. Biol. Chem.* **277**:9268–9277.
17. Seta, K., and Sadoshima, J. 2003. Phosphorylation of tyrosine 319 of the AT1 receptor mediates angiotensin II-induced trans-activation of the EGF receptor. *J. Biol. Chem.* **269**:9019–9026.
18. Sadoshima, J. 1998. Versatility of the AT1 receptor. *Circ. Res.* **82**:1352–1355.
19. Ali, M.S., et al. 1997. Dependence on the motif YIPP for the physical association of Jak2 kinase with the intracellular carboxyl tail of the angiotensin II AT1 receptor. *J. Biol. Chem.* **272**:23382–23388.
20. Venema, R.C., et al. 1998. Angiotensin II-induced association of phospholipase Cgamma1 with the G-protein-coupled AT1 receptor. *J. Biol. Chem.* **273**:7703–7708.
21. Marrero, M.B., et al. 1995. Direct stimulation of Jak/STAT pathway by the angiotensin II AT1 receptor. *Nature.* **375**:247–250.
22. Marrero, M.B., Venema, V.J., Ju, H., Eaton, D.C., and Venema, R.C. 1998. Regulation of angiotensin II-induced JAK2 tyrosine phosphorylation: roles of SHP-1 and SHP-2. *Am. J. Physiol.* **275**:C1216–C1223.
23. Lopez-Ilasaca, M., Liu, X., Tamura, K., and Dzau, V.J. 2003. The angiotensin II type I receptor-associated protein, ATRAP, is a transmembrane protein and a modulator of angiotensin II signaling. *Mol. Biol. Cell.* **14**:5038–5050.
24. Molkentin, J.D., and Dorn, I.G., 2nd. 2001. Cytoplasmic signaling pathways that regulate cardiac hypertrophy. *Annu. Rev. Physiol.* **63**:391–426.
25. Sakata, Y., Hoit, B.D., Liggett, S.B., Walsh, R.A., and Dorn, G.W.I. 1998. Decompensation of pressure overload hypertrophy in Gαq-overexpressing mice. *Circulation.* **97**:1488–1496.
26. Shioi, T., et al. 2000. The conserved phosphoinositide 3-kinase pathway determines heart size in mice. *EMBO J.* **19**:2537–2548.
27. Bueno, O.F., et al. 2000. The MEK1-ERK1/2 signaling pathway promotes compensated cardiac hypertrophy in transgenic mice. *EMBO J.* **19**:6341–6350.
28. Ernst, O.P., Hofmann, K.P., and Sakmar, T.P. 1995. Characterization of rhodopsin mutants that bind transducin but fail to induce GTP nucleotide uptake. Classification of mutant pigments by fluorescence, nucleotide release, and flash-induced light-scattering assays. *J. Biol. Chem.* **270**:10580–10586.
29. Ohyama, K., Yamano, Y., Chaki, S., Kondo, T., and Inagami, T. 1992. Domains for G-protein coupling in angiotensin II receptor type I: studies by site-directed mutagenesis. *Biochem. Biophys. Res. Commun.* **189**:677–683.
30. Kupershmidt, S., et al. 1999. Replacement by homologous recombination of the minK gene with lacZ reveals restriction of minK expression to the mouse cardiac conduction system. *Circ. Res.* **84**:146–152.
31. Pashmforoush, M., et al. 2004. Nkx2-5 pathways and congenital heart disease; loss of ventricular myocyte lineage specification leads to progressive cardiomyopathy and complete heart block. *Cell.* **117**:373–386.
32. Irisawa, H., Brown, H.F., and Giles, W. 1993. Cardiac pacemaking in the sinoatrial node. *Physiol. Rev.* **73**:197–227.
33. Platzer, J., et al. 2000. Congenital deafness and sinoatrial node dysfunction in mice lacking class D L-type Ca2+ channels. *Cell.* **102**:89–97.
34. Zhang, Z., et al. 2002. Functional roles of Ca(v)1.3 (alpha(1D)) calcium channel in sinoatrial nodes: insight gained using gene-targeted null mutant mice. *Circ. Res.* **90**:981–987.
35. Formstecher, E., et al. 2001. PEA-15 mediates cytoplasmic sequestration of ERK MAP kinase. *Dev. Cell.* **1**:239–250.
36. Kubes, M., Cordier, J., Glowinski, J., Girault, J.A., and Chneiweiss, H. 1998. Endothelin induces a calcium-dependent phosphorylation of PEA-15 in intact astrocytes: identification of Ser104 and Ser116 phosphorylated, respectively, by protein kinase C and calcium/calmodulin kinase II in vitro. *J. Neurochem.* **71**:1307–1314.
37. Zou, Y., et al. 2004. Mechanical stress activates angiotensin II type 1 receptor without the involvement of angiotensin II. *Nat. Cell Biol.* **6**:499–506.
38. Bockaert, J., and Pin, J.P. 1999. Molecular tinkering of G protein-coupled receptors: an evolutionary success. *EMBO J.* **18**:1723–1729.
39. Hall, R.A., Premont, R.T., and Lefkowitz, R.J. 1999. Heptahelical receptor signaling: beyond the G protein paradigm. *J. Cell Biol.* **145**:927–932.
40. Milligan, G., and White, J.H. 2001. Protein-protein interactions at G-protein-coupled receptors. *Trends Pharmacol. Sci.* **22**:513–518.
41. Marinissen, M.J., and Gutkind, J.S. 2001. G-protein-coupled receptors and signaling networks: emerging paradigms. *Trends Pharmacol. Sci.* **22**:368–376.
42. Sah, V.P., et al. 1999. Cardiac-specific overexpression of RhoA results in sinus and atrioventricular nodal dysfunction and contractile failure. *J. Clin. Invest.* **103**:1627–1634.
43. Nakamura, K., et al. 2001. Complete heart block and sudden death in mice overexpressing calreticulin. *J. Clin. Invest.* **107**:1245–1253.
44. Fabritz, L., et al. 2004. Gene dose-dependent atrial arrhythmias, heart block, and brady-cardiomyopathy in mice overexpressing A(3) adenosine receptors. *Cardiovasc. Res.* **62**:500–508.
45. Modrall, J.G., et al. 2001. ANG II type 1 receptor downregulation does not require receptor endocytosis or G protein coupling. *Am. J. Physiol. Cell Physiol.* **281**:C801–C809.
46. George, S.R., O'Dowd, B.F., and Lee, S.P. 2002. G-protein-coupled receptor oligomerization and its potential for drug discovery. *Nat. Rev. Drug Discov.* **1**:808–820.
47. AbdAlla, S., Lother, H., and Quitterer, U. 2000. AT1-receptor heterodimers show enhanced G-protein activation and altered receptor sequestration. *Nature.* **407**:94–98.
48. Ito, M., et al. 1995. Regulation of blood pressure by the type 1A angiotensin II receptor gene. *Proc. Natl. Acad. Sci. U. S. A.* **92**:3521–3525.
49. Hirotani, S., et al. 2004. Ca(2+)-sensitive tyrosine kinase Pyk2/CAK beta-dependent signaling is essential for G-protein-coupled receptor agonist-induced hypertrophy. *J. Mol. Cell. Cardiol.* **36**:799–807.
50. Fuller, S.J., Gillespie-Brown, J., and Sugden, P.H. 1998. Oncogenic src, raf, and ras stimulate a hypertrophic pattern of gene expression and increase cell size in neonatal rat ventricular myocytes. *J. Biol. Chem.* **273**:18146–18152.
51. Torsoni, A.S., Constancio, S.S., Nadruz, W., Jr., Hanks, S.K., and Franchini, K.G. 2003. Focal adhesion kinase is activated and mediates the early hypertrophic response to stretch in cardiac myocytes. *Circ. Res.* **93**:140–147.
52. Hein, L., et al. 1997. Overexpression of angiotensin AT1 receptor transgene in the mouse myocardium produces a lethal phenotype associated with myocyte hyperplasia and heart block. *Proc. Natl. Acad. Sci. U. S. A.* **94**:6391–6396.
53. Allen, A.M., Yamada, H., and Mendelsohn, F.A. 1990. In vitro autoradiographic localization of binding to angiotensin receptors in the rat heart. *Int. J. Cardiol.* **28**:25–33.
54. Sechi, L.A., Griffin, C.A., Grady, E.F., Kalinyak, J.E., and Schambelan, M. 1992. Characterization of angiotensin II receptor subtypes in rat heart. *Circ. Res.* **71**:1482–1489.
55. De Mello, W.C. 1994. Is an intracellular renin-angiotensin system involved in control of cell communication in heart? *J. Cardiovasc. Pharmacol.* **23**:640–646.
56. Redfern, C.H., et al. 1999. Conditional expression and signaling of a specifically designed Gi-coupled receptor in transgenic mice. *Nat. Biotechnol.* **17**:165–169.
57. Aiello, E.A., and Cingolani, H.E. 2001. Angiotensin II stimulates cardiac L-type Ca(2+) current by a Ca(2+)- and protein kinase C-dependent mechanism. *Am. J. Physiol. Heart Circ. Physiol.* **280**:H1528–H1536.
58. De Mello, W.C., and Monterrubio, J. 2004. Intracellular and extracellular angiotensin II enhance the L-type calcium current in the failing heart. *Hypertension.* **44**:360–364.
59. Adams, J.W., and Brown, J.H. 2001. G-proteins in growth and apoptosis: lessons from the heart. *Oncogene.* **20**:1626–1634.
60. Yussman, M.G., et al. 2002. Mitochondrial death protein Nix is induced in cardiac hypertrophy and triggers apoptotic cardiomyopathy. *Nat. Med.* **8**:725–730.
61. Vaidyanathan, H., and Ramos, J.W. 2003. RSK2 activity is regulated by its interaction with PEA-15. *J. Biol. Chem.* **278**:32367–32372.
62. Alcendor, R.R., Kirshenbaum, L.A., Imai, S., and Sadoshima, J. 2004. Sir2α, a longevity factor and a class III histone decetylase, is an essential endogenous inhibitor of apoptosis in cardiac myocytes. *Circ. Res.* **95**:971–980.
63. Hardt, S.E., Tomita, H., Katus, H.A., and Sadoshima, J. 2004. Phosphorylation of eukaryotic translation initiation factor 2Bepsilon by glycogen synthase kinase-3beta regulates beta-adrenergic cardiac myocyte hypertrophy. *Circ. Res.* **94**:926–935.
64. Paridis, P., Dali-Youcef, N., Paradis, F.W., Thibault, G., and Nemer, M. 2000. Overexpression of angiotensin II type I receptor in cardiomyocytes induces cardiac hypertrophy and remodeling. *Proc. Natl. Acad. Sci. U. S. A.* **97**:931–936.
65. Yamamoto, S., et al. 2003. Activation of Mst1 causes dilated cardiomyopathy by stimulating apoptosis without compensatory ventricular myocyte hypertrophy. *J. Clin. Invest.* **111**:1463–1474. doi:1172/JCI200317459.
66. Masaki, H., Sato, Y., Luo, W., Kranias, E.G., and Yatani, A. 1997. Phospholamban deficiency alters inactivation kinetics of L-type Ca2+ channels in mouse ventricular myocytes. *Am. J. Physiol.* **272**:H606–H612.
67. Yatani, A., Frank, K., Sako, H., Kranias, E.G., and Dorn, G.W., 2nd. 1999. Cardiac-specific overexpression of Galphaq alters excitation-contraction coupling in isolated cardiac myocytes. *J. Mol. Cell. Cardiol.* **31**:1327–1336.
68. Ping, P., et al. 1999. PKC-dependent activation of p44/p42 MAPKs during myocardial ischemia-reperfusion in conscious rabbits. *Am. J. Physiol.* **276**:H1468–H1481.